Mechanism of Oxygen Reduction Reaction on Transition Metal-Nitrogen-Carbon Catalysts: Establishing the Role of Nitrogen-containing Active Sites

Yechuan Chen,[†,‡] Ivana Matanovic,[†,+] Elizabeth Weiler,[†] Plamen Atanassov[†] and Kateryna Artyushkova[,†,‡]*

[†]Department of Chemical and Biological Engineering, Center for Micro-Engineered Materials (CMEM), University of New Mexico, Albuquerque, New Mexico 87131, United States

[+]Theoretical Division, Los Alamos National Laboratory, Los Alamos, New Mexico 87545, United States

Keywords: transition metal-nitrogen-carbon catalyst • oxygen reduction reaction • catalyst inhibition • catalyst active sites probing • near ambient pressure XPS • mechanism of ORR • DFT calculations • spectroscopic probes.

ABSTRACT: Using molecular probes that have unique spectral signatures and have strong selective binding to the potential active sites allows elucidating the mechanism of different reactions. The mechanism of oxygen reduction reaction in metal-nitrogen-carbon (MNC) catalysts has been studied by using a bisphosphonate complexing agent, which improves the selectivity of

ORR by blocking the protonated and hydrogenated nitrogen that are catalyzing the partial reduction of oxygen to hydrogen peroxide. A combination of theoretical, electrochemical and spectroscopic with focus on Near-ambient pressure X-ray Photoelectron Spectroscopy is used to directly probe the competition between binding of oxygen and molecular probe to the surface of MNC catalyst and to identify the role of different types of nitrogen in the mechanism of ORR.

The mechanism of oxygen reduction reaction (ORR) in metal-nitrogen-carbon (MNC) catalysts have been studied extensively by a combination of spectroscopic and theoretical structure-to-activity studies. [1-12] Heterogeneous nature of MNC catalysts, in which a multitude of active nitrogen species participating in different stages of oxygen reduction reaction exist, complicates enumeration of active site density. One of the strategies to investigate the mechanism of oxygen reduction reaction occurring via either direct 4-electron transfer or via $2\times2e^-$ reduction is the use of reactive probes that have selectivity towards binding to different types of structural motifs present in MNC material. Molecular probes, such as cyanide and carbon monoxide, have been used to poison active catalytic sites in rotating disk electrode (RDE) measurements. [9, 13-20] Recently, Mamtani et al. have shown that phosphate anion is selective towards binding to pyridinic nitrogen. [19] Another protocol was introduced that allows the quantification of active centers using nitrile adsorption followed by reductive stripping. [18] Spectroscopy can be used as an objective confirmatory tool for the selective binding of probes to certain chemical moieties. For example, NO in combination with Mössbauer and NMR spectroscopy has been routinely used as a probe to iron active sites. [16]

In addition to challenge in finding probes that are selective, it is also desirable for them to be spectroscopically distinguishable from the spectral signature of the catalyst itself. Majority of

complexing agents that can be used as probes are nitrogen-based. One of the types of complexing agents free of nitrogen is a bisphosphonate chelating agent 1-hydroxyethane 1,1-diphosphonic acid (HEDP).

Based on DFT calculations published previously, multiple types of nitrogen existing in the MNC materials show strong binding of reactants, intermediates, ionomers and other adsorbates that can be used as molecular probes and inhibitors. [13, 21-22] For example, sulfonate group of ionomers shows strong binding with Fe-N_x and weaker but still very significant binding to both graphitic and hydrogenated nitrogen active sites. [22] On the other hand, oxygen has the strongest binding to Fe-N_x centers and weaker binding to other types of nitrogen. [21] Recently, we have introduced an inhibitor based on tris(hydroxyl-methyl)-aminomethane (Tris) that shows strongest binding to pyridinic and slightly weaker binding to Fe-N_x centers.

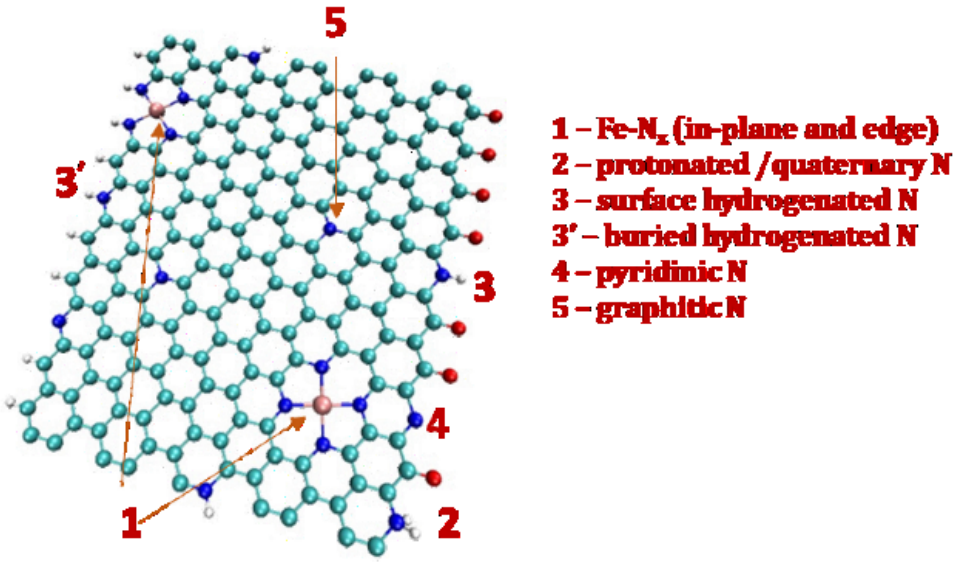

Figure 1. The types of chemical moieties present in the MNC catalyst.

The multiple nitrogen sites existing in the MNC catalysts discussed in detail in multiple previous reports are summarized in Figure 1. First, multiple types of nitrogen coordinated with iron in either

in-plane mesomeric Fe-N_4 ***(1)*** or edge disordered Fe-N_x (x<4) configuration are present. Edge sites include pyridinic N ***(4)***, hydrogenated N ***(3)*** and quaternary N ***(2)***. Hydrogenated N includes both pyrrolic and hydrogenated pyridine. Pyridine can also be present in protonated form with positive charge. In-plane graphitic N can be present as in-plane defect ***(5)*** with or without proton depending on the local pH environment.[2]

Table 1 compares the adsorption energies of oxygen, sulfonate fragment of Nafion, TrisH (protonated Tris) inhibitor reported recently, and HEDP on different types of nitrogen and Fe-N_x moieties shown in Figure S4 as computed by DFT. Figure 2 shows structures with HEDP fragment (in the mono-deprotonated form as its pK_{a1} is 1.35) adsorbed. The results reported corresponds to the orientation and configuration with the largest adsorption energy. HEDP has strong adsorption energies to most of the nitrogen types with the highest affinity to Fe-N_x sites. Moreover, the adsorption energy of HEDP onto quaternary nitrogen which encompasses any types of nitrogen that are protonated [23] (edge quaternary nitrogen, in-plane protonated graphitic nitrogen, and protonated pyridinic nitrogen) has the largest value of -3.79 eV (not listed in Table 1).

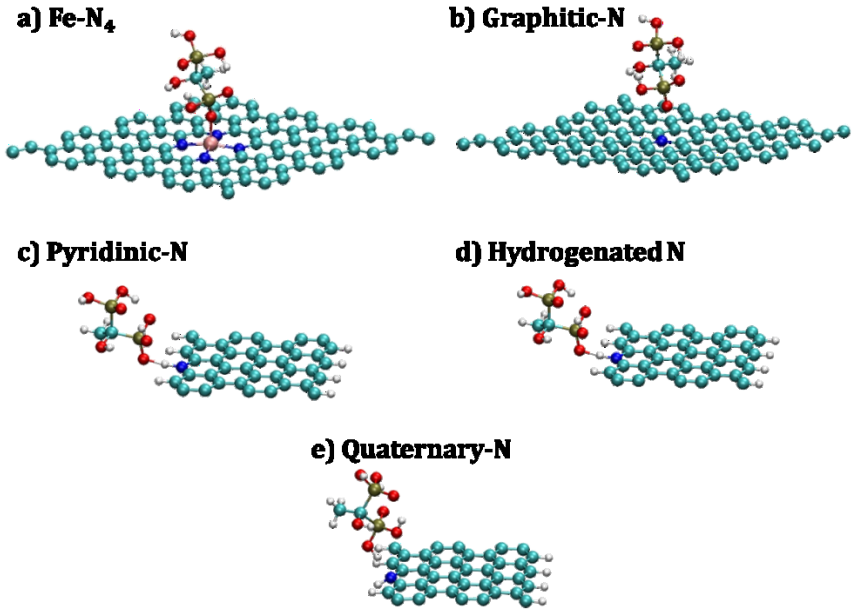

Figure 2. DFT optimized geometries of deprotonated HEDP adsorbed on (a) Fe-N_x, (b) graphitic N, (c) pyridinic-N, (d) hydrogenated pyridinic-N and (e) quaternary-N. Atoms belonging to one unit cell are shown. Blue – N, white – H, red – O, tan – P, cyan – C, pink – Fe.

Table 1. Adsorption energy of assorted active sites with different molecules, in the unit of eV. HEDP is in the first acid dissociated form.

Site	O_2	SO_3	TrisH	HEDP
Fe-N_x	-1.01 [24] to -1.43 [21]	-3.3 [22]	-1.96 (x=4) [13]	-2.18
Graphitic-N	-0.13 [24] to -0.41 [21]	-1.9 [22]	-1.07 [13]	-1.49
Pyridinic-N	-0.08 [24] to -0.28 [21]	-0.9 [22]	-3.65 [13]	-0.88
Hydrogenated pyridinic-N / Pyrrolic-N	-0.21 [24] to -0.25 [21]	-2.25 [22]	-0.53 [13]	-1.53

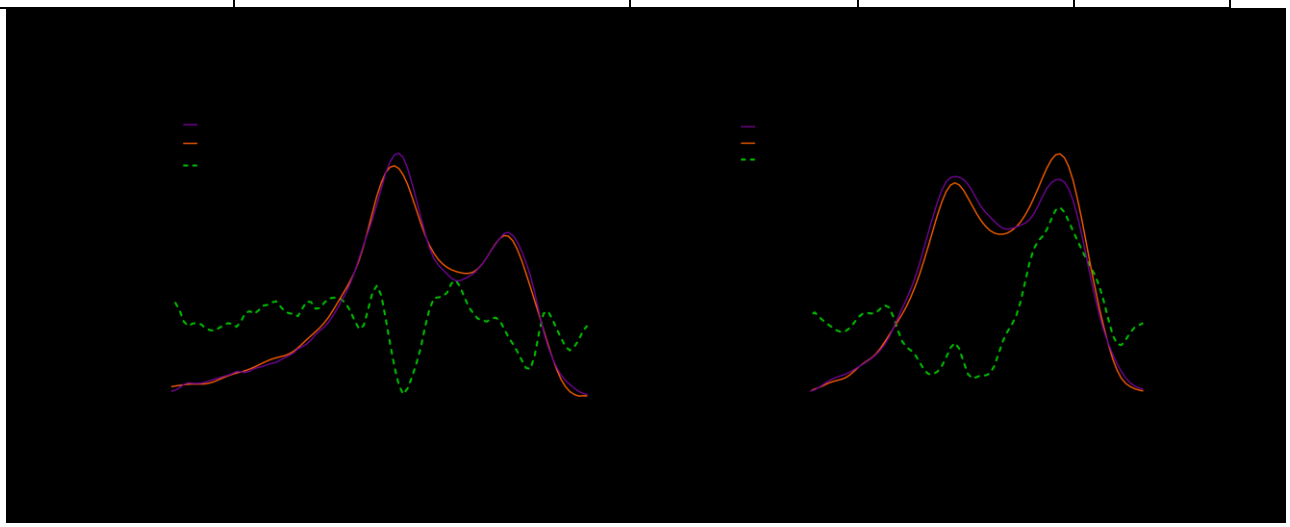

Figure 3. High-resolution N 1s spectra for fresh catalyst and catalyst after exposure and washing away HEDP overlayed spectra and difference spectra for (a) 1000 eV N 1s photoelectron and (b) 150 eV N 1s electron. Fitted spectra are shown in Figure S1, while quantitative information showing relative at % of peak components is shown in Table 2.

To confirm the binding of HEDP to the surface of the catalyst, spectroscopic analysis of changes in the surface chemistry of catalyst upon exposure and after washing of HEDP was performed by high-resolution XPS. The surface chemistry of pure catalyst and the catalyst after its exposure to HEDP at two different sampling depths was studied by both a fixed source lab-based and variable energy synchrotron-based instrument. In the lab-based instrument N 1s photoelectron has a kinetic energy of 1000 eV and it originates from approximately 20 nm of the surface, while in a synchrotron-based instrument N 1s photoelectron has a kinetic energy of only 150 eV originating from the surface depth of 2.5 nm. The power of energy-variable XPS using synchrotron sources at different source energies was demonstrated previously for another sample from the same family of materials.[21] After washing HEDP from the surface of the catalyst, 0.5 at% of P is detected confirming its irreversible binding to the surface. Due to surface sensitivity of XPS, mostly unbound HEDP is detected for the unwashed sample with P 2p having single peak due to free phosphonate groups at 133.5 eV. After washing away HEDP, there is a shift in the position of P 2p peak to lower binding energy of 132.7 eV (Figure S2) due to phosphonate complexation with functional groups of the catalyst. A small amount of unbound phosphonate is still observed at the surface. Figure 3 shows high-resolution N 1s spectra from both sampling depths for pure catalyst and catalyst with bound HEDP, while Table 2 shows the relative surface chemical composition of nitrogen. There is a smaller amount of N detected at the surface (2.7 at % at 2 nm vs. 3.7 at % at 20 nm) which may be due to the actual smaller concentration of nitrogen present or due to a larger amount of oxygen originating from surface carbon oxide groups. The relative distribution of nitrogen provides reliable and relevant information on differences in chemical composition at different sampling depths.

Table 2. Quantitative analysis showing relative speciation of nitrogen species for pure catalyst and catalyst after exposure to HEDP and their difference for two experimental conditions, at synchrotron and at the lab-based spectrometer obtained by fitting the spectra as shown in Figure S1.

Kinetic energy, Sampling depth	***398.4 eV***	***399.5 eV***	***400.8 eV***	***401.8 eV***	***402.9 eV***
150 eV 2.6 nm	N_{pyr} (4)	N_x-Fe (1)	N-H (3)	N^+/N_{gr} (2,5)	NO/ Bulk N-H (3')
Catalyst	32.6	20.3	32.5	12.0	2.7
Catalyst +HEDP washed	36.2	20.5	30.7	9.6	3.1
Difference	*3.6*	*0.2*	*-1.8*	*-2.4*	*0.4*
	398.4 eV	***399.5 eV***	***400.8 eV***	***401.8 eV***	***402.9 eV***
1000 eV 20 nm	N_{pyr} (4)	N_x-Fe (1)	N-H (3)	N^+/N_{gr} (2,5)	NO/ Bulk N-H (3')
Catalyst	25.1	15.5	32.8	14.6	12.0
Catalyst +HEDP washed	25.8	14.8	31.3	13.7	14.4
Difference	*0.7*	*-0.7*	*-1.6*	*-0.8*	*1.2*

The abbreviation of pyr and gr means pyridinic and graphitic respectively. The numbers in brackets point to Figure 1.

Very different distribution of nitrogen species at different sampling depths is evident in the catalyst. Closer to the surface, a higher concentration of edge pyridinic nitrogen groups is detected. The peak at 399.5 eV has contribution from different types of iron coordinated to nitrogen, including in-plane mesomeric Fe-N_4 moieties and disordered edge sites such as Fe-N, Fe-N_2 and Fe-N_3.[25] Mesomeric Fe-N_4 moieties are located within the plane of graphene layer, while those coordinated to smaller than 4 nitrogen are expected to be located at the edge of exposed graphene plane. [26] A larger concentration of N_x-Fe closer to the surface confirms the hypothesis that the

species contributing to peak at 399.5 eV are not only mesomeric symmetrical in-plane Fe-N_4 centers, but also disordered Fe-N_x sites that are predominantly present at the edges and exposed more to the surface.[25] At deeper sampling depth, there is also the more significant contribution of the peak at a binding energy of 403 eV. The hydrogenated pyridinic and pyrrolic nitrogen N-H edge defects located closer to the surface/air interface and therefore terminated with oxygenated carbon contribute to binding energy of 400.8 eV, while the N 1s binding energy of the same defects in network terminated with hydrogen (C-H) is much higher at ~403 eV.[23, 27] The difference in the relative abundance of the high binding energy peak at 403 eV for two different sampling depths confirms that hydrogenated nitrogen atoms located at deeper depths are surrounded by a mixture of graphitic and amorphous aliphatic carbons contributing to the energy of 403 eV. Figure 3 shows the structure of nitrogen moieties as discussed.

The changes in nitrogen chemistry when the catalyst is exposed to HEDP is captured by the difference spectra between the fresh catalyst and after exposure to the adsorbate (Figure 3). The difference in spectra within deeper layers is less pronounced due to a smaller fraction of the signal coming from the adsorbed HEDP to the total 20 nm sampling depth. The difference spectra visualize major trends in the spectral shifts with and without the adsorbates. At the same time, the quantitative changes in distribution of surface concentrations of nitrogen species can be investigated based on curve fits of the spectra as shown in Figure S1. There is a decrease in the relative amount of edge hydrogenated nitrogen and protonated nitrogen, particularly closer to the surface. Deprotonated HEDP has a very high adsorption energy to these sites, and during the DFT optimization, it is observed that H is transferred from quaternary-N to HEDP. After washing the catalyst+HEDP with deionized water, HEDP should be removed, and protonated pyridinic nitrogen should be converted to pyridinic-N. This prediction is confirmed by an increase in the relative

amount of unprotonated pyridines (peak at 398.4 eV) after washing away the HEDP as shown in Table 2. No significant difference in the region of the peak due to Fe-N_x (399.5 eV) is observed. The smaller decrease in the amount of protonated nitrogen in the deeper probed layers (peak at 401.8 eV) may indicate that these nitrogen atoms are not in-plane protonated graphitic N but edge surface defects such as quaternary and protonated pyridines. From the spectroscopic analysis of catalyst with and without adsorbed HEDP, it can be concluded that the major sites blocked by HEDP are hydrogenated and protonated nitrogen atoms

To probe the effect of the inhibitor onto the oxygen reduction reaction, linear sweep voltammetry (LSV) in 0.5 M sulfuric acid was performed using a rotating ring disk electrode (RRDE) (Figure 4). Half-wave potentials of pure catalyst, the catalyst in the presence of 0.3 M HEDP and catalyst after washing HEDP with deionized water for 15 minutes are almost the same, being 0.72V. Figure S5 shows that this behavior is true even for higher concentrations of HEDP up to 1.0 M. There is a drop of disk current density in diffusion region at 0.2 V from 4.15 mA cm^{-2} in the pure catalyst to 3.41 mA cm^{-2} in the presence of 0.3 M HEDP, which is completely recovered after washing inhibitor away. According to the previous study, at the concentrations of inhibitor larger than 0.1M there is a decreased oxygen solubility causing a decrease in the current density in diffusion-limited regime. [28] Figure S6 shows that the calculated number of electrons involved in the reaction does not depend on the presence of HEDP. This behavior indicates that HEDP doesn't compete with oxygen for binding to sites catalyzing full 4 electron reduction of oxygen to water.

On the other hand, there is a significant effect of HEDP onto the ring current density, which decreases from 0.029 mA cm^{-2} for a pure catalyst to 0.013 mA cm^{-2} for a catalyst with HEDP added (values at 0.6 V). This can be mainly attributed to the inhibition of sites that mainly contribute to partial 2-e^- reduction of oxygen into hydrogen peroxide. Based on DFT data and spectroscopic

data discussed above, these sites are surface hydrogenated nitrogen and protonated nitrogen. After washing HEDP away, there is a partial recovery of ring current density to 0.019 mA cm-2, indicating that HEDP binding to hydrogenated and protonated nitrogen sites is not completely reversible. Based on a combination of spectroscopic analysis and RRDE studies, we can conclude that there is selective inhibition of nitrogen active sites responsible for the partial reduction of oxygen to hydrogen peroxide. Similar values of the slope of Tafel plots calculated for three tests in Figure 4 (98.16, 94.83 and 99.89 mV dec-1 for the pure electrolyte, 0.3M HEDP and refreshed electrolyte, respectively) confirm that HEDP does not affect iron-nitrogen active sites responsible for the full reduction of oxygen to water.

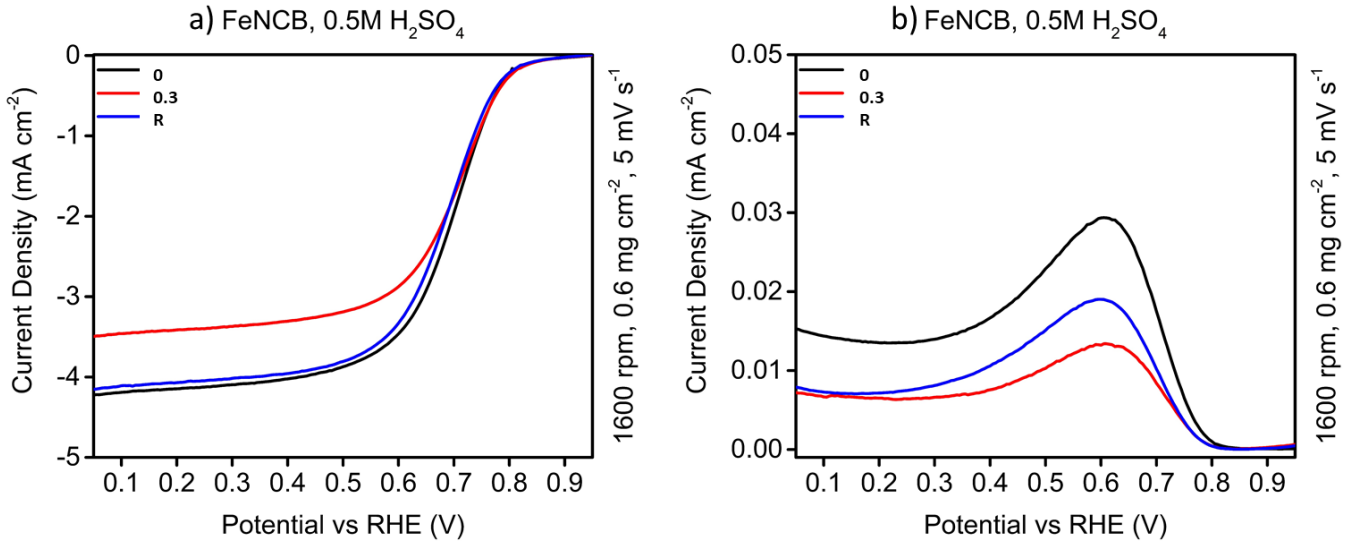

Figure 4. LSV data of catalyst tested in 0.5 M sulfuric acid, (a) disk current density and (b) ring current density. Legends of 0, 0.3 and R mean pure electrolyte, 0.3 M HEDP added and refreshed electrolyte. Corresponding parameters are 0.6 mg cm^{-2} loading of catalyst, 1600 rpm of rotation speed and 5 mV s^{-1} of scanning rate. The metrics of performance, i.e. half-way potential, ring and disk current densities are discussed in text.

To directly demonstrate how oxygen adsorption is affected by the presence of HEDP, near ambient pressure XPS (NAPXPS) was performed for in-situ spectroscopic characterization. Figure S3 shows high-resolution O 1s spectra acquired in the gaseous atmosphere for both samples showing that in addition to gaseous water and oxygen phase there is the presence of bound hydroxyls and oxygen at the surface. Figure 5 shows high-resolution N 1s spectra for the pure catalyst and catalyst with adsorbed HEDP at UHV conditions and after exposure to the O_2/H_2O atmosphere. The difference spectra are plotted as well. The negative values in the difference spectra represent decrease in the intensity of peaks due to species which bind oxygen and hydroxyls to it. For quantitative analysis of spectroscopic changes occurring at the surface of catalyst upon exposure to humidified oxygen gas we referred to the results of curve fit of N 1s spectra in Figure 5 as summarized in Table 3. In the case of a pure catalyst, there is a decrease in the relative amounts of peaks due to N_x-Fe and N^+/N_{gr} moieties seen in both Table 3 and highlighted negative peaks in difference spectra. These observations are consistent with a previously published report showing the duality of sites for oxygen binding in MNC catalysts dependent on the strength of oxygen binding to different nitrogen species. [11] The oxygen binding to the catalyst with adsorbed HEDP results in very different behavior. The large difference in lower binding energy of N 1s spectrum around 399 eV is observed in the negative part of the difference spectra highlighted in green in Figure 5 b indicating binding of oxygen to N_x-Fe sites and pyridinic nitrogen. Binding of oxygen and water to Nx-Fe sites causes the shift of the peak at 399.5 eV to higher binding energy causing an increase in the relative abundance of the peak at 400.8 eV. Binding of water to pyridinic nitrogen causes its protonation contributing to an increase in the peak 401.8 eV. No binding to protonated and graphitic nitrogen is detected at higher binding energy as these sites are blocked by adsorbed HEDP.

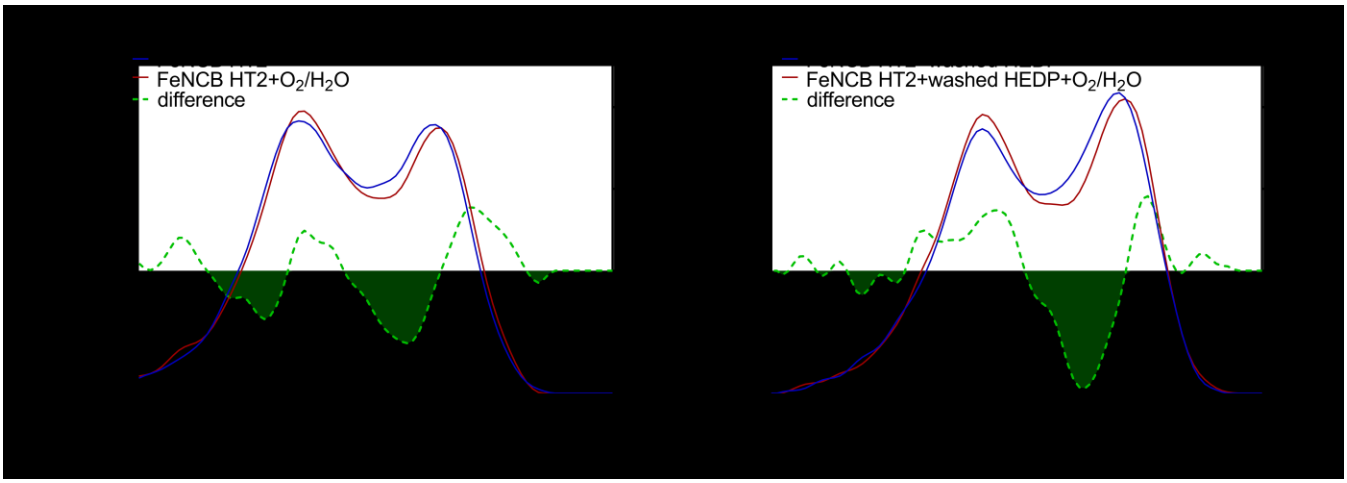

Figure 5. High-resolution N 1s spectra and difference spectra for the fresh catalyst (a) and catalyst after exposure and washing away HEDP overlayed (b) in UHV and in 200 mtorr of oxygen and water (1:1 volume ratio). Quantitative information showing relative at % of peak components and change in it upon exposure to oxygen is shown in Table 3.

Table 3. Relative speciation of nitrogen species for pure catalyst and catalyst after exposure to HEDP in UHV and a gaseous environment. The difference between them for two experimental conditions is shown.

	398.4 eV	***399.5 eV***	***400.8 eV***	***401.8 eV***	***402.9 eV***
FeNCB	N_{pyr} (4)	N_x-Fe (1)	N-H (3)	N^+/N_{gr} (2,5)	NO/ Bulk N-H (3')
Catalyst UHV	32.6	20.3	32.5	12.0	2.7
Catalyst +gas	32.8	18.4	33.6	10.9	4.3
Difference	*0.2*	*-1.8*	*1.1*	*-1.1*	*1.6*
	398.4 eV	***399.5 eV***	***400.8 eV***	***401.8 eV***	***402.9 eV***
FeNCB + washed HEDP	N_{pyr} (4)	N_x-Fe (1)	N-H (3)	N^+/N_{gr} (2,5)	NO/

					Bulk N-H (3')
Catalyst + washed HEDP UHV	36.2	20.5	30.7	9.6	3.1
Catalyst + washed HEDP +gas	34.2	19.1	33.5	10.9	2.4
Difference	*-2.0*	*-1.4*	*2.8*	*1.3*	*-0.7*

The numbers in brackets point to Figure 1.

The results of the in-situ spectroscopy and electrochemical testing, therefore, clearly identify the chemical structures that are responsible for two parallel mechanisms of ORR, via direct 4 electron reduction of oxygen to water, which occurs on iron coordinated to nitrogen Fe-N_x sites, and via dual site 2×2 electron mechanism, where protonated and hydrogenated nitrogen catalyze the reduction of oxygen to hydrogen peroxide. [29] From previous studies, we have observed that pyridinic nitrogen is catalyzing the second step of reaction of H_2O_2 reduction to H_2O. [11] The role of different defects in the ORR mechanism on MNC catalysts are illustrated in Figure 6.

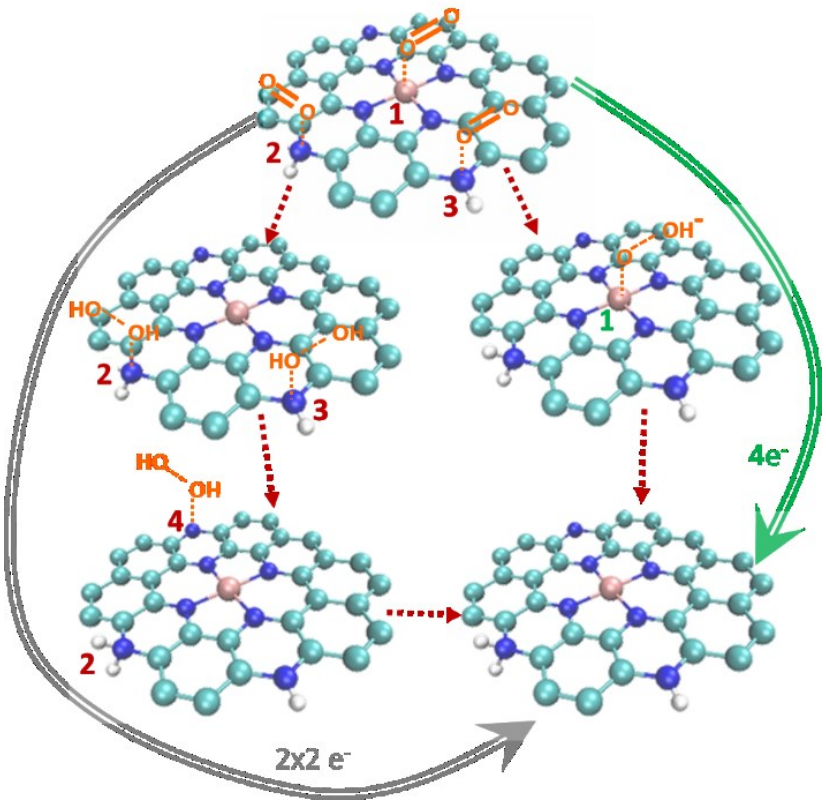

Figure 6. Two parallel pathways of ORR mechanism are shown. Oxygen binds strongly to N_x-Fe(1), N-H (3) and N^+ (2) sites. Direct $4e^-$ occurs on N_x-Fe sites, while N-H and N^+ catalyze $2e^-$ reduction to H_2O_2 which is further reduced on pyridinic N

In conclusion, the HEDP is a unique inhibitor that has strong and partially irreversible adsorption to protonated and hydrogenated nitrogen, which increases the selectivity of the catalyst towards the 4-electron reduction of oxygen to water. HEDP has, therefore, a potential application as fuel cell cathode additive to improve cathode selectivity. Importantly, selectivity of HEDP towards binding to hydrogen peroxide producing sites should ensure that total density of sites performing full oxygen reduction to water will not be reduced.

ASSOCIATED CONTENT

Supporting Information

Methods for synthesis, electrochemistry measurements, XPS data collection and DFT calculation, XPS figures

AUTHOR INFORMATION

Corresponding Author

*kartyush@unm.edu

Author Contributions

The manuscript was written through contributions of all authors. All authors have given approval to the final version of the manuscript. ‡These authors contributed equally.

Funding Sources

NSF award # 1738386 RII Track-4: Operando Analysis of Fuel Cell Materials at Advanced Light Source.

ACKNOWLEDGMENT

The Advanced Light Source is supported by the Director, Office of Science, Office of Basic Energy Sciences, of the U.S. Department of Energy under Contract No. DE-AC02-05CH11231. I.G. thankfully acknowledges the computational resources from the Tri-Lab computing resources of LANL, operated by Los Alamos National Security, LLC, for the National Nuclear Security Administration of U.S. Department of Energy (Contract DE-AC52-06NA25396), NERSC, a DOE Office of Science User Facility supported by the Office of Science of the U.S. Department of Energy under Contract No. DE-AC02-05CH11231, and CNMS, which is a DOE Office of Science

User Facility. VASP license was provided by Theoretical Division, LANL. This paper has been designated LA-UR-18-24832.

REFERENCES

(1) Singh, K.; Razmjooei, F.; Yu, J.-S. Active Sites and Factors Influencing them for Efficient Oxygen Reduction Reaction in Metal-N Coordinated Pyrolyzed and Non-pyrolyzed Catalysts: A Review. *Journal of Materials Chemistry A* **2017,** *5*, 20095-20119.

(2) Rojas-Carbonell, S.; Artyushkova, K.; Serov, A.; Santoro, C.; Matanovic, I.; Atanassov, P. Effect of pH on the Activity of Platinum Group Metal-Free Catalysts in Oxygen Reduction Reaction. *ACS Catalysis* **2018**, *8*, 3041-3053.

(3) Wang, T.; Chen, Z.-X.; Chen, Y.-G.; Yang, L.-J.; Yang, X.-D.; Ye, J.-Y.; Xia, H.-P.; Zhou, Z.-Y.; Sun, S.-G. Identifying the Active Site of N-Doped Graphene for Oxygen Reduction by Selective Chemical Modification. *ACS Energy Letters* **2018**, *3*, 986-991.

(4) Xing, T.; Zheng, Y.; Li, L. H.; Cowie, B. C. C.; Gunzelmann, D.; Qiao, S. Z.; Huang, S.; Chen, Y. Observation of Active Sites for Oxygen Reduction Reaction on Nitrogen-Doped Multilayer Graphene. *ACS Nano* **2014,** *8*, 6856-6862.

(5) Chai, G.-L.; Hou, Z.; Shu, D.-J.; Ikeda, T.; Terakura, K. Active Sites and Mechanisms for Oxygen Reduction Reaction on Nitrogen-Doped Carbon Alloy Catalysts: Stone–Wales Defect and Curvature Effect. *Journal of the American Chemical Society* **2014,** *136*, 13629-13640.

(6) Jaouen, F.; Proietti, E.; Lefevre, M.; Chenitz, R.; Dodelet, J.-P.; Wu, G.; Chung, H. T.; Johnston, C. M.; Zelenay, P. Recent Advances in Non-precious Metal Catalysis for Oxygen-reduction Reaction in Polymer Electrolyte Fuel Cells. *Energy & Environmental Science* **2011,** *4*, 114-130.

(7) Varnell, J. A.; Sotiropoulos, J. S.; Brown, T. M.; Subedi, K.; Haasch, R. T.; Schulz, C. E.; Gewirth, A. A. Revealing the Role of the Metal in Non-Precious-Metal Catalysts for Oxygen Reduction via Selective Removal of Fe. *ACS Energy Letters* **2018**, *3*, 823-828.

(8) Ramaswamy, N.; Mukerjee, S. Influence of Inner- and Outer-Sphere Electron Transfer Mechanisms during Electrocatalysis of Oxygen Reduction in Alkaline Media. *The Journal of Physical Chemistry C* **2011,** *115*, 18015-18026.

(9) Zitolo, A.; Goellner, V.; Armel, V.; Sougrati, M.-T.; Mineva, T.; Stievano, L.; Fonda, E.; Jaouen, F. Identification of Catalytic Sites for Oxygen Reduction in Iron- and Nitrogen-doped Graphene Materials. *Nat Mater* **2015,** *14*, 937-942,.

(10) Yang, Z.; Yao, Z.; Li, G.; Fang, G.; Nie, H.; Liu, Z.; Zhou, X.; Chen, X. a.; Huang, S. Sulfur-Doped Graphene as an Efficient Metal-free Cathode Catalyst for Oxygen Reduction. *ACS Nano* **2012,** *6*, 205-211.

(11) Artyushkova, K.; Serov, A.; Rojas-Carbonell, S.; Atanassov, P. Chemistry of Multitudinous Active Sites for Oxygen Reduction Reaction in Transition Metal–nitrogen–carbon Electrocatalysts. *The Journal of Physical Chemistry C* **2015,** *119*, 25917-25928.

(12) Jia, Q.; Ramaswamy, N.; Tylus, U.; Strickland, K.; Li, J.; Serov, A.; Artyushkova, K.; Atanassov, P.; Anibal, J.; Gumeci, C.; Barton, S. C.; Sougrati, M.-T.; Jaouen, F.; Halevi, B.; Mukerjee, S. Spectroscopic Insights into the Nature of Active Sites in Iron–nitrogen–carbon Electrocatalysts for Oxygen Reduction in Acid. *Nano Energy* **2016,** *29*, 65-82.

(13) Chen, Y.; Artyushkova, K.; Rojas-Carbonell, S.; Serov, A.; Matanovic, I.; Santoro, C.; Asset, T.; Atanassov, P. Inhibition of Surface Chemical Moieties by Tris(hydroxymethyl)aminomethane: A Key to Understanding Oxygen Reduction on Iron–Nitrogen–Carbon Catalysts. *ACS Applied Energy Materials* **2018,** *1*, 1942-1949.

(14) Chung, H. T.; Cullen, D. A.; Higgins, D.; Sneed, B. T.; Holby, E. F.; More, K. L.; Zelenay, P. Direct Atomic-level Insight into the Active Sites of a High-performance PGM-free ORR Catalyst. *Science* **2017,** *357*, 479-484.

(15) Chung, M. W.; Chon, G.; Kim, H.; Jaouen, F.; Choi, C. H. Electrochemical Evidence for Two Sub-families of FeNxCy Moieties with Concentration-Dependent Cyanide Poisoning. *ChemElectroChem* **2018,** *5*, 1880-1885.

(16) Kneebone, J. L.; Daifuku, S. L.; Kehl, J. A.; Wu, G.; Chung, H. T.; Hu, M. Y.; Alp, E. E.; More, K. L.; Zelenay, P.; Holby, E. F.; Neidig, M. L. A Combined Probe-Molecule, Mössbauer, Nuclear Resonance Vibrational Spectroscopy, and Density Functional Theory Approach for Evaluation of Potential Iron Active Sites in an Oxygen Reduction Reaction Catalyst. *The Journal of Physical Chemistry C* **2017,** *121*, 16283-16290.

(17) Leonard, N. D.; Wagner, S.; Luo, F.; Steinberg, J.; Ju, W.; Weidler, N.; Wang, H.; Kramm, U. I.; Strasser, P. Deconvolution of Utilization, Site Density, and Turnover Frequency of Fe–Nitrogen–Carbon Oxygen Reduction Reaction Catalysts Prepared with Secondary N-Precursors. *ACS Catalysis* **2018**, *8*, 1640-1647.

(18) Malko, D.; Kucernak, A.; Lopes, T. In situ Electrochemical Quantification of Active sites in Fe–N/C Non-precious Metal Catalysts. *Nature Communications* **2016,** *7*, 13285.

(19) Mamtani, K.; Jain, D.; Zemlyanov, D.; Celik, G.; Luthman, J.; Renkes, G.; Co, A. C.; Ozkan, U. S. Probing the Oxygen Reduction Reaction Active Sites over Nitrogen-Doped Carbon Nanostructures (CNx) in Acidic Media Using Phosphate Anion. *ACS Catalysis* **2016,** *6*, 7249-7259.

(20) Thorum, M. S.; Hankett, J. M.; Gewirth, A. A. Poisoning the Oxygen Reduction Reaction on Carbon-Supported Fe and Cu Electrocatalysts: Evidence for Metal-Centered Activity. *The Journal of Physical Chemistry Letters* **2011,** *2*, 295-298.

(21) Artyushkova, K.; Matanovic, I.; Halevi, B.; Atanassov, P. Oxygen Binding to Active Sites of Fe–N–C ORR Electrocatalysts Observed by Ambient-Pressure XPS. *The Journal of Physical Chemistry C* **2017,** *121*, 2836-2843.

(22) Artyushkova, K.; Workman, M. J.; Matanovic, I.; Dzara, M. J.; Ngo, C.; Pylypenko, S.; Serov, A.; Atanassov, P. Role of Surface Chemistry on Catalyst/Ionomer Interactions for Transition Metal–Nitrogen–Carbon Electrocatalysts. *ACS Applied Energy Materials* **2018,** *1*, 68-77.

(23) Matanovic, I.; Artyushkova, K.; Strand, M. B.; Dzara, M. J.; Pylypenko, S.; Atanassov, P. Core Level Shifts of Hydrogenated Pyridinic and Pyrrolic Nitrogen in the Nitrogen-Containing Graphene-Based Electrocatalysts: In-Plane vs Edge Defects. *The Journal of Physical Chemistry C* **2016,** *120*, 29225-29232.

(24) Sebastián, D.; Serov, A.; Matanovic, I.; Artyushkova, K.; Atanassov, P.; Aricò, A. S.; Baglio, V. Insights on the Extraordinary Tolerance to Alcohols of Fe-N-C Cathode Catalysts in Highly Performing Direct Alcohol Fuel Cells. *Nano Energy* **2017,** *34*, 195-204.

(25) Artyushkova, K.; Serov, A.; Rojas-Carbonell, S.; Atanassov, P. Chemistry of Multitudinous Active Sites for Oxygen Reduction Reaction in Transition Metal–Nitrogen–Carbon Electrocatalysts. *J. Phys. Chem. C* **2015,** *119*, 25917–25928.

(26) Workman, M. J.; Serov, A.; Tsui, L.-k.; Atanassov, P.; Artyushkova, K. Fe–N–C Catalyst Graphitic Layer Structure and Fuel Cell Performance. *ACS Energy Letters* **2017,** *2* (7), 1489-1493, DOI: 10.1021/acsenergylett.7b00391.

(27) Matanovic, I.; Artyushkova, K.; Atanassov, P. Understanding PGM-free Catalysts by Linking Density Functional Theory Calculations and Structural Analysis: Perspectives and Challenges. *Current Opinion in Electrochemistry* **2018**, *9*, 137-144.

(28) Chen, Y.; Artyushkova, K.; Rojas-Carbonell, S.; Serov, A.; Matanovic, I.; Santoro, C.; Asset, T.; Atanassov, P. Inhibition of Surface Chemical Moieties by Tris(hydroxymethyl)aminomethane: A Key to Understanding Oxygen Reduction on Iron–Nitrogen–Carbon Catalysts. *ACS Applied Energy Materials* **2018**, *1* (5), 1942–1949, DOI: 10.1021/acsaem.8b00020.

(29) Tylus, U.; Jia, Q.; Strickland, K.; Ramaswamy, N.; Serov, A.; Atanassov, P.; Mukerjee, S. Elucidating Oxygen Reduction Active Sites in Pyrolyzed Metal–Nitrogen Coordinated Non-Precious-Metal Electrocatalyst Systems. *The Journal of Physical Chemistry C* **2014,** *118* (17), 8999-9008, DOI: 10.1021/jp500781v.

Establishing the Role of Nitrogen-containing Active Sites in Oxygen Reduction Reaction